Vol 463|14 January 2010|doi:10.1038/nature08705

LETTERS

Three-dimensional structure determination from a single view

Kevin S. Raines[1,2], Sara Salha[1,2], Richard L. Sandberg[4,5], Huaidong Jiang[1,2], Jose A. Rodríguez[3], Benjamin P. Fahimian[1,2], Henry C. Kapteyn[4,5], Jincheng Du[6,7] & Jianwei Miao[1,2]

The ability to determine the structure of matter in three dimensions has profoundly advanced our understanding of nature. Traditionally, the most widely used schemes for three-dimensional (3D) structure determination of an object are implemented by acquiring multiple measurements over various sample orientations, as in the case of crystallography and tomography[1,2], or by scanning a series of thin sections through the sample, as in confocal microscopy[3]. Here we present a 3D imaging modality, termed ankylography (derived from the Greek words *ankylos* meaning 'curved' and *graphein* meaning 'writing'), which under certain circumstances enables complete 3D structure determination from a single exposure using a monochromatic incident beam. We demonstrate that when the diffraction pattern of a finite object is sampled at a sufficiently fine scale on the Ewald sphere, the 3D structure of the object is in principle determined by the 2D spherical pattern. We confirm the theoretical analysis by performing 3D numerical reconstructions of a sodium silicate glass structure at 2 Å resolution, and a single poliovirus at 2–3 nm resolution, from 2D spherical diffraction patterns alone. Using diffraction data from a soft X-ray laser, we also provide a preliminary demonstration that ankylography is experimentally feasible by obtaining a 3D image of a test object from a single 2D diffraction pattern. With further development, this approach of obtaining complete 3D structure information from a single view could find broad applications in the physical and life sciences.

Lensless imaging techniques generally begin with the coherent diffraction pattern of a non-crystalline sample, which is measured and then directly phased to obtain an image. The initial insight that the continuous diffraction pattern of a non-crystalline object might be invertible was suggested in 1980 (ref. 4). In 1999, coherent diffraction microscopy was first experimentally demonstrated[5]. Since that initial demonstration, lensless imaging has advanced considerably, and has been applied to a wide range of samples, including nanoparticles, nanocrystals, biomaterials, cells, cellular organelles, viruses and carbon nanotubes by synchrotron radiation[6–19], electrons[20,21], high harmonic and short wavelength laser sources[22,23], and free electron lasers[24–26]. However, in order to generate 3D images by coherent diffraction microscopy, multiple diffraction patterns are required at different sample orientations[7,10–13,16,19]. The precise mechanical tilting necessary to obtain these patterns or the requirement of having multiple identical copies of the specimen[27] prevents 3D imaging by a single X-ray free electron laser (X-FEL) pulse or time-resolved 3D structure determination of disordered materials. Here we develop a novel imaging modality—ankylography—that could overcome these limitations (although it introduces additional constraints that may not always be satisfied).

Figure 1 shows a schematic layout of the conceptual set-up for ankylography. A coherent beam of wavelength λ illuminates a finite object. The scattered waves form a diffraction pattern on the Ewald sphere, which can be expressed in the spherical polar coordinate system (Supplementary Discussion) as:

$$|F(\theta,\phi)| = \left| \int_V \rho(\mathbf{r}) e^{-\frac{2\pi i}{\lambda}[x\sin\theta\cos\phi + y\sin\theta\sin\phi + z(\cos\theta - 1)]} d^3\mathbf{r} \right| \quad (1)$$

where $|F(\theta,\phi)|$ is proportional to the magnitude of the scattered waves, θ and φ are the spherical polar coordinates, $\rho(\mathbf{r})$ the 3D structure of the object with $\mathbf{r} = (x, y, z)$, and V the spatial extent of the object. When the 2D spherical diffraction pattern is sampled at a scale sufficiently finer than the Nyquist interval such that the oversampled degree (O_d) is larger than 1, the oversampled diffraction pattern in principle determines the 3D structure of the object (Supplementary Discussion), which can be retrieved by iterative algorithms. Here O_d is defined as the ratio of the number of measured intensity points from equation (1) to the number of unknown variables of the 3D object array[28]. Although equation (1) assumes plane wave illumination, ankylography can be extended to divergent or convergent wave illumination through deconvolution with the illumination function. The 3D spatial resolution of ankylography is determined by (Supplementary Fig. 1):

$$d_x = d_y = \frac{\lambda}{\sin(2\theta_{\max})} \qquad d_z = \frac{\lambda}{2\sin^2\theta_{\max}} \quad (2)$$

where d_x, d_y and d_z represent the resolution along the x, y and z axes, respectively. The z axis is along the beam propagation direction, and $2\theta_{\max}$ is the diffraction angle shown in Fig. 1.

To confirm our theoretical analysis, we conducted numerical simulations of 3D structure determination of sodium silicate glasses ($25Na_2O$-$75SiO_2$). Sodium silicate glasses are archetypal for a wide variety of multicomponent silicate glasses that find applications from glassware and window panes, to optical fibres, photonic devices and bioactive glasses. Unlike crystalline materials, glasses lack long-range periodicity, which makes experimental determination of the glass structure difficult by traditional diffraction methods. Thus the inherent complexity of glass structures combined with the lack of experimental methods to probe them (especially for medium range structures) makes understanding and visualizing the atomic and nanostructure of glasses a great challenge to the scientific community. By combining classical molecular dynamics (MD) simulations with subsequent geometry optimization using *ab initio* density functional theory calculations, we obtained a 3D sodium silicate glass structure of 204 atoms, with a size of $14 \times 14 \times 14$ Å (Supplementary Methods). A beam of coherent X-rays with a wavelength of 2 Å was incident on the nanostructure. The total coherent flux illuminating the glass structure was

[1]Department of Physics and Astronomy, [2]California NanoSystems Institute, [3]Molecular Biology Institute, University of California, Los Angeles, California 90095, USA. [4]Department of Physics, [5]JILA, University of Colorado, Boulder, Colorado 80309, USA. [6]Department of Materials Science & Engineering, [7]Center for Advanced Scientific Computing and Modeling, University of North Texas, Denton, Texas 76203, USA.

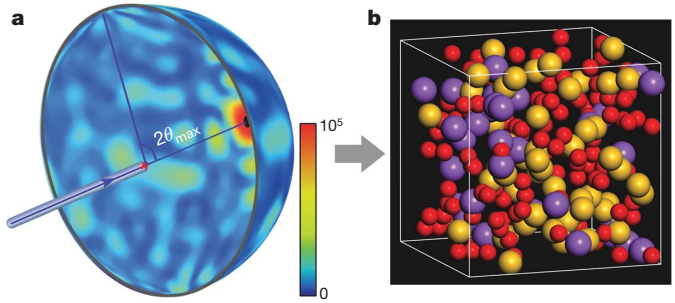

Figure 1 | Schematic layout of the conceptual set-up for ankylography. A coherent beam illuminates a finite object and the scattered waves form a diffraction pattern on the Ewald sphere (**a**), where $2\theta_{max}$ represents the diffraction angle. When the diffraction pattern is sampled at a scale sufficiently finer than the Nyquist interval, the 3D structure of the object is in principle encoded into the 2D spherical pattern and can be directly reconstructed (**b**). Here, the 3D object is a sodium silicate glass particle with a size of $14 \times 14 \times 14$ Å. The red, purple and yellow spheres represent the positions of O, Na and Si atoms, respectively. Colour scale in **a** shows number of photons.

about 10^{13} photons. An oversampled 2D diffraction pattern was calculated on the Ewald sphere, with $2\theta_{max} = 90^\circ$. Poisson noise was added to the spherical diffraction pattern, shown in Fig. 1a.

To reconstruct the 3D glass structure, we embedded the 2D spherical diffraction pattern into a 3D array of $64 \times 64 \times 64$ voxels, corresponding to $O_d = 2.7$. As the electron density of the glass structure is real, we also embedded the centro-symmetrical diffraction pattern into the same array. All other data points in the 3D array were set as unknowns. The 3D reconstruction was computed using a phase retrieval algorithm which iterated back and forth between Fourier and real space (Methods Summary and Supplementary Discussion). In Fourier space, the measured data points on the Ewald sphere were updated in each iteration. In real space, the non-zero values outside the envelope of the 3D structure (that is, a support) were suppressed. In addition, we also exploited the fact that the region outside the support should be uniform. Inside the support, we enforced the constraint that the electron density must be non-negative and continuous (details of the constraints and the phase retrieval algorithm can be found in Supplementary Discussion). Figure 1b shows the 3D atomic positions of the reconstructed sodium silicate glass structure with a resolution of 2 Å in all three dimensions (see Supplementary Fig. 2 for resolution quantification). In Fig. 1b, the red, purple and yellow spheres represent the positions of O, Na and Si atoms, respectively. Compared to the MD simulated structure, the 3D atomic positions of the sodium silicate glass structure are resolved. Figure 2 shows two 2-Å-thick slices of the MD simulations (Fig. 2a and c) and the reconstructed structures (Fig. 2b and d) along the x–y and x–z planes, respectively. The electron density distribution of the reconstructed structure is in good agreement with that of the MD simulation. The slight difference of the electron density between the two structures is likely to be due to the Poisson noise added to the diffraction pattern.

To explore theoretically the biological application of ankylography, we performed a numerical experiment on 3D image reconstruction of an individual poliovirus from a single X-FEL pulse. Poliovirus contains a single-stranded RNA genome within an icosahedral capsid that is delivered into a host cell via interaction of virus coat proteins with a poliovirus receptor[29]. During this process, the virus undergoes an irreversible conformational change that results in an increased affinity for the poliovirus receptor, producing what is known as the 135S particle[29]. In the numerical experiment, we simulated an X-FEL pulse with $\lambda = 1.77$ nm and 10^{13} photons per pulse that was focused to a 100 nm spot and illuminated a single 135S particle. The 3D model structure of the poliovirus has been obtained by cryo-electron microscopy through averaging 8,224 particles[29]. A diffraction pattern on the Ewald sphere was obtained with a diffraction angle of 62.6°, which

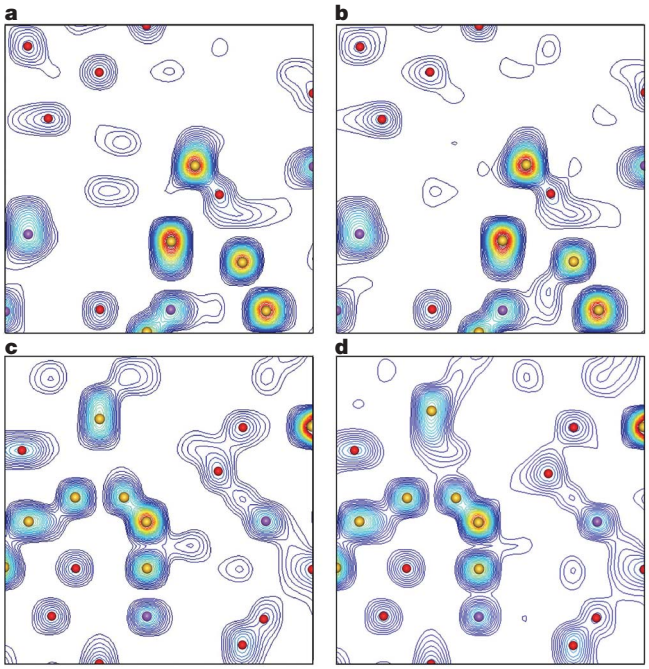

Figure 2 | 3D structure determination of a sodium silicate glass particle at 2 Å resolution from a simulated 2D spherical diffraction pattern alone. **a**, **b**, Electron density distribution of a 2-Å-thick slice of the MD simulation (**a**) and the reconstructed structure (**b**) along the x–y plane, where the red, purple and yellow spheres represent the positions of O, Na and Si atoms, respectively. **c**, **d**, Electron density distribution of a 2-Å-thick slice of the MD simulation (**c**) and the reconstructed structure (**d**) along the x–z plane. The width and height of each slice are 14 Å.

corresponds to a spatial resolution of 2.0 nm in the x–y plane and 3.3 nm along the z axis. Poisson noise was added to the diffraction intensities. The 3D ankylographic reconstruction was computed using the iterative algorithm without a priori information of the virus structure (Methods Summary and Supplementary Discussion). We also noted that when the array size of the 3D object becomes larger, the ankylographic reconstruction requires additional constraints. In the reconstruction of the poliovirus, we applied not only the constraints of uniformity outside the support, continuity inside the support and non-negativity of the electron density, but also the amplitude extension constraint (that is, gradually computing the 3D reconstruction from low to high resolutions; see Supplementary Discussion for details).

Figure 3a and b shows an iso-surface rendering and a 1.65-nm-thick central slice of the 3D virus structure reconstructed from the 2D

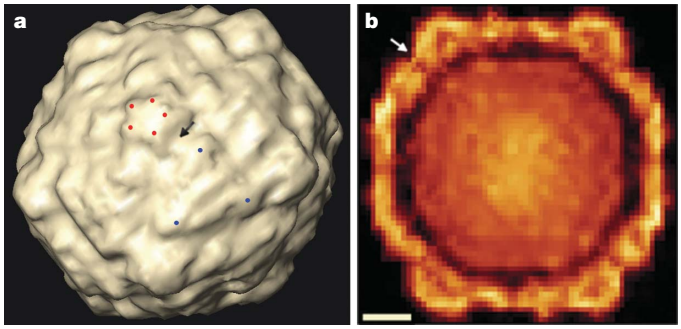

Figure 3 | 3D structure determination of an individual poliovirus from a single simulated X-FEL pulse. **a**, Iso-surface rendering of the reconstructed viral capsid structure, showing a five-fold mesa (red dots) and the tips of a three-fold propeller (blue dots). The canyon between the mesa and the propeller structure (arrowed) is the expected binding site to its receptor. **b**, A 1.65-nm-thick central slice of the reconstructed 3D virus structure across the five-fold mesa and the propeller structure. The arrow indicates the receptor binding site. Scale bar, 5 nm.

noisy diffraction pattern alone, which are in excellent agreement with the model (Supplementary Fig. 3). The reconstructed 3D capsid structure clearly resolves the star-shaped mesa that forms the five-fold symmetry (red dots in Fig. 3a) and the propeller tips (blue dots in Fig. 3a) that form the three-fold symmetry. In the vicinity of the five-fold mesa and the propeller structure is a canyon (indicated with arrows in Fig. 3a and b), which is the expected binding site of the poliovirus receptor. Compared to cryo-electron microscopy, which enables 3D imaging of large protein complexes such as viruses by averaging over thousands of particles, ankylography can potentially be used to determine the 3D structure of a single biological complex at high resolution.

As an initial attempt to verify ankylography with experimental data, we used a 2D diffraction pattern taken with a soft X-ray laser of $\lambda = 47$ nm and $\lambda/\Delta\lambda \approx 10^4$ (ref. 24). The test pattern was fabricated by etching through a substrate consisting of a silicon nitride membrane of thickness ~100 nm. Except for the patterned area, the substrate was opaque to the 47 nm light. A slant of the test sample relative to the incident beam served to increase the z-axis width of the sample, providing a 3D depth (Fig. 4b). The CCD detector (Andor, 2,048 × 2,048 pixel extreme ultraviolet detector array, 13.5 × 13.5 μm^2 pixel size) was positioned at a distance of 14.5 mm from the sample. A 2D diffraction pattern was measured by the detector with intensities extending to the edges of the CCD camera. To enhance the signal to noise ratio, we integrated the diffraction intensities by binning 3 × 3 pixels into 1 pixel and then interpolated the planar diffraction pattern onto the Ewald sphere (Supplementary Discussion, Fig. 4a). The spherical diffraction pattern was embedded into a 3D array of 420 × 420 × 240 voxels with $O_d = 2.6$.

The phase retrieval was carried out using similar methods to those used for the sodium silicate glass structure (Methods Summary and Supplementary Discussion). Figure 4b and c shows iso-surface renderings of the 3D reconstruction in the x–y plane (front view) and the x–z plane (side view), respectively, in which the front view is in good agreement with the scanning electron microscopy (SEM) image (Fig. 4e). The spatial resolution of the reconstructed image was estimated to be 80 nm along the x and y axes and 140 nm along the z axis. On the basis of the 3D reconstruction, we measured the tilt angle of the sample relative to the beam to be 5.1° (Fig. 4b). Figure 4d shows a line scan along the z axis of the reconstructed image. The width of the tilted sample's projection onto the z axis was measured to be 405 nm in the reconstruction, which is in good agreement with the expected value of 389 nm computed from the sample geometry and the tilt angle. Moreover, we identified two structure defects in the test sample, which were present in the SEM image taken after the experiment (arrows in Fig. 4e), but not in the SEM image before the experiment. These structure defects, which were probably due to dust particles deposited on the edge of the sample, are spatially resolved in the 3D reconstructed image (arrows in Fig. 4b). Although our reconstruction agrees well with the 3D structure of the test sample, we acknowledge that this is probably a non-ideal test sample, for the following reasons. First, the sample was relatively thin and, even after tilting, the z-axis width was still a few times smaller than the dimensions in other axes. Second, it was a transparent sample on an opaque substrate, which potentially lends itself to other interpretations[30,31]. It is hence desirable to have more convincing experiments in the future.

In conclusion, we have discovered that the 3D structure information of a finite object is in principle encoded into a 2D diffraction pattern on the Ewald sphere. When the diffraction pattern is sufficiently oversampled, the 3D structure may be directly retrieved from the 2D spherical diffraction pattern using the phase retrieval algorithm with physical constraints. Both our numerical simulations and preliminary experimental results have indicated the feasibility of this 3D imaging technique. Compared to conventional 3D coherent diffraction microscopy[7,10–13,16,19], ankylography requires a comparable amount of incident flux for achieving a desired resolution, but redistributes all the intensities more finely on the Ewald sphere, which eliminates the necessity of sample tilting. On the other hand, ankylography requires additional constraints to facilitate the 3D reconstruction from spherical diffraction pattern alone.

Although we have applied the constraints of non-negativity, uniformity outside the support, continuity inside the support and amplitude extension in this study, there are more physical constraints that may be used to further improve the ankylographic reconstructions; these include atomicity[1], histogram matching[1], molecular replacement[1] and non-crystallographic symmetry[1]. Furthermore, owing to the oversampling requirement of the single 2D diffraction pattern, ankylography demands area detectors with a large number of pixels to compute 3D reconstructions of sizeable specimens at high resolutions. In addition, to reduce the interpolation errors (Supplementary Discussion), spherical area detectors are more desirable in ankylography. Finally, our preliminary numerical simulations have indicated that, with two or more 2D spherical diffraction patterns, the 3D image reconstruction can be distinctively improved. Thus ankylography may also be used to reduce the number of tilts required in 3D coherent diffraction microscopy. Looking forward, by incorporating

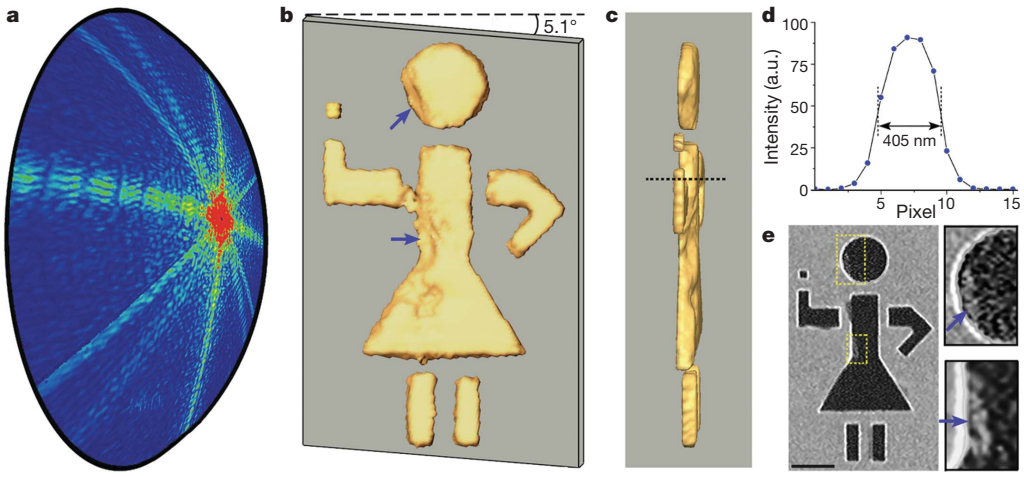

Figure 4 | Demonstration of ankylography using experimental data obtained with a soft X-ray laser. **a**, Oversampled 2D diffraction pattern on the Ewald sphere. **b**, **c**, Iso-surface renderings of the 3D reconstructed image in the x–y plane (**b**) and the x–z plane (**c**), where the incident beam is along the z axis. **d**, Line scan taken along the dashed line in **c** indicates the width of the tilted sample's projection onto the z axis to be 405 nm. **e**, SEM image of the sample (scale bar, 1 μm). Insets (right) show two structure defects (arrowed) in the sample which are spatially resolved in the 3D reconstructed image (arrows in **b**).

additional constraints into the phase retrieval algorithm and using dedicated detectors, ankylography could be applied to perform 3D structure determination of a broad range of specimens without the necessity of sample tilting, scanning or sectioning.

METHODS SUMMARY

3D image reconstruction in ankylography proceeds by means of an iterative algorithm. A random phase set defines an initial input and iterates back and forth between Fourier and real space where physical constraints were applied. In Fourier space, the magnitudes of the Fourier transform on the Ewald sphere were set to the measured values. The data points not on the Ewald sphere were initially set as unknowns and updated with each iteration of the reconstruction. In real space, the following constraints were enforced: the electron density must be non-negative, continuous, and bounded within a support. Data points of the image estimate that did not satisfy the positivity or boundedness constraints were modified by the operations described further in Supplementary Information. In order to enforce continuity of the image within the support, a Gaussian filter was periodically applied to the image density throughout the reconstruction. Outside the support, where the density should be uniform, in addition to approximately zero-valued, convolution with a box kernel was implemented as described in Supplementary Information. An error metric, defined as the difference between the computed data points on the Ewald sphere and the measured ones, was used to monitor the convergence of the algorithm.

In order to capitalize on the fast convergence of the 3D reconstructions, where knowledge of a tight support is not necessary, we begin with a low-resolution reconstruction in order to recover the missing magnitudes in Fourier space. We subsequently include these recovered amplitudes in the higher resolution reconstructions. We call this type of constraint 'amplitude extension'. This constraint allows the object envelope to be easily computed without a priori information. A detailed description of how these constraints are implemented can be found in Supplementary Information.

Received 3 May; accepted 25 November 2009.
Published online 16 December 2009.

1. Giacovazzo, C. *et al. Fundamentals of Crystallography* 2nd edn (Oxford Univ. Press, 2002).
2. Kak, A. C. & Slaney, M. *Principles of Computerized Tomographic Imaging* (SIAM, 2001).
3. Pawley, J. B. (ed.) *Handbook of Biological Confocal Microscopy* 3rd edn (Springer, 2006).
4. Sayre, D. in *Imaging Processes and Coherence in Physics* (eds Schlenker, M. *et al.*) 229–235 (Lecture Notes in Physics, Vol. 112, Springer, 1980).
5. Miao, J., Charalambous, P., Kirz, J. & Sayre, D. Extending the methodology of X-ray crystallography to allow imaging of micrometre-sized non-crystalline specimens. *Nature* **400,** 342 (1999).
6. Robinson, I. K., Vartanyants, I. A., Williams, G. J., Pfeifer, M. A. & Pitney, J. A. Reconstruction of the shapes of gold nanocrystals using coherent X-ray diffraction. *Phys. Rev. Lett.* **87,** 195505 (2001).
7. Miao, J. *et al.* High resolution 3D X-ray diffraction microscopy. *Phys. Rev. Lett.* **89,** 088303 (2002).
8. Miao, J. *et al.* Imaging whole *Escherichia coli* bacteria by using single-particle x-ray diffraction. *Proc. Natl Acad. Sci. USA* **100,** 110–112 (2003).
9. Nugent, K. A., Peele, A. G., Chapman, H. N. & Mancuso, A. P. Unique phase recovery for nonperiodic objects. *Phys. Rev. Lett.* **91,** 203902 (2003).
10. Shapiro, D. *et al.* Biological imaging by soft x-ray diffraction microscopy. *Proc. Natl Acad. Sci. USA* **102,** 15343–15346 (2005).
11. Pfeifer, M. A., Williams, G. J., Vartanyants, I. A., Harder, R. & Robinson, I. K. Three-dimensional mapping of a deformation field inside a nanocrystal. *Nature* **442,** 63–66 (2006).
12. Miao, J. *et al.* Three-dimensional GaN-Ga_2O_3 core shell structure revealed by x-ray diffraction microscopy. *Phys. Rev. Lett.* **97,** 215503 (2006).
13. Chapman, H. N. *et al.* High resolution *ab initio* three-dimensional x-ray diffraction microscopy. *J. Opt. Soc. Am. A* **23,** 1179–1200 (2006).
14. Williams, G. J. *et al.* Fresnel coherent diffractive imaging. *Phys. Rev. Lett.* **97,** 025506 (2006).
15. Abbey, B. *et al.* Keyhole coherent diffractive imaging. *Nature Phys.* **4,** 394–398 (2008).
16. Jiang, H. *et al.* Nanoscale imaging of mineral crystals inside biological composite materials using X-ray diffraction microscopy. *Phys. Rev. Lett.* **100,** 038103 (2008).
17. Thibault, P. *et al.* High-resolution scanning X-ray diffraction microscopy. *Science* **321,** 379–382 (2008).
18. Song, C. *et al.* Quantitative imaging of single, unstained viruses with coherent X-rays. *Phys. Rev. Lett.* **101,** 158101 (2008).
19. Nishino, Y., Takahashi, Y., Imamoto, N., Ishikawa, T. & Maeshima, K. Three-dimensional visualization of a human chromosome using coherent X-ray diffraction. *Phys. Rev. Lett.* **102,** 018101 (2009).
20. Zuo, J. M., Vartanyants, I., Gao, M., Zhang, R. & Nagahara, L. A. Atomic resolution imaging of a carbon nanotube from diffraction intensities. *Science* **300,** 1419–1421 (2003).
21. Spence, J. C. H., Weierstall, U. & Howells, M. R. Phase recovery and lensless imaging by iterative methods in optical, X-ray and electron diffraction. *Phil. Trans. R. Soc. Lond. A* **360,** 875–895 (2002).
22. Sandberg, R. L. *et al.* Lensless diffractive imaging using tabletop coherent high-harmonic soft-X-ray beams. *Phys. Rev. Lett.* **99,** 098103 (2007).
23. Sandberg, R. L. *et al.* High numerical aperture tabletop soft X-ray diffraction microscopy with 70 nm resolution. *Proc. Natl Acad. Sci. USA* **105,** 24–27 (2008).
24. Chapman, H. N. *et al.* Femtosecond diffractive imaging with a soft-X-ray free-electron laser. *Nature Phys.* **2,** 839–843 (2006).
25. Barty, A. *et al.* Ultrafast single-shot diffraction imaging of nanoscale dynamics. *Nature Photon.* **2,** 415–419 (2008).
26. Mancuso, A. P. *et al.* Coherent-pulse 2D crystallography using a free-electron laser X-ray source. *Phys. Rev. Lett.* **102,** 035502 (2009).
27. Neutze, R., Wouts, R., Spoel, D., Weckert, E. & Hajdu, J. Potential for biomolecular imaging with femtosecond X-ray pulses. *Nature* **406,** 752–757 (2000).
28. Miao, J., Sayre, D. & Chapman, H. N. Phase retrieval from the magnitude of the Fourier transforms of non-periodic objects. *J. Opt. Soc. Am. A* **15,** 1662–1669 (1998).
29. Bubeck, D. *et al.* The structure of the poliovirus 135S cell entry intermediate at 10-Angstrom resolution reveals the location of an externalized polypeptide that binds to membranes. *J. Virol.* **79,** 7745–7755 (2005).
30. Thibault, P. Feasibility of 3D reconstruction from a single 2D diffraction measurement. Preprint at ⟨http://arXiv.org/abs/0909.1643v1⟩ (2009).
31. Miao, J. Response to feasibility of 3D reconstruction from a single 2D diffraction measurement. Preprint at ⟨http://arXiv.org/abs/0909.3500v1⟩ (2009).

Supplementary Information is linked to the online version of the paper at www.nature.com/nature.

Acknowledgements We thank P. Thibault for commenting on our manuscript, P. Thibault, M. M. Murnane, C.-C. Chen and R. Fung for discussions, C. Song for performing data analysis, Y. Mao for implementing an interpolation code, A. E. Sakdinawat for fabricating a test sample, P. Wachulak, M. Marconi, C. Menoni, J. J. Rocca and M. M. Murnane for help with data acquisition and T. Singh for parallelization of our phase retrieval codes. This work was supported by the US DOE, Office of Basic Energy Sciences, and the US NSF, Division of Materials Research and Engineering Research Center, an HHMI Gilliam fellowship for advanced studies and the UCLA MBI Whitcome fellowship. We used facilities supported by the NSF Center in EUV Science and Technology.

Author Contributions J.M. and K.S.R. conceived of ankylography. J.M. planned the project; K.S.R., S.S., H.J., J.A.R., J.D. and J.M. conducted the numerical experiments; S.S., K.S.R., R.L.S., H.J., H.C.K. and J.M. performed the analysis and image reconstruction of experimental data; J.M., K.S.R, S.S., J.D. and J.A.R. wrote the manuscript. All authors discussed the results and commented on the manuscript.

Author Information Reprints and permissions information is available at www.nature.com/reprints. The authors declare no competing financial interests. Correspondence and requests for materials should be addressed to J.M. (miao@physics.ucla.edu).